Research Square

Preprints are preliminary reports that have not undergone peer review.
They should not be considered conclusive, used to inform clinical practice,
or referenced by the media as validated information.

Endoscopic NIRAF-LSCI Multimodal System with Pseudo-Color Visualization for Parathyroid Autofluorescence Localization and Tissue Perfusion Assessment: Preclinical Validation

Chang Cai
Guangzhou Medical University
Chuoqi Yang
Guangzhou Medical University
Wanyu Sun
Guangzhou Medical University
Qiye Wen
Guangzhou Medical University
Xiao Xiao
Guangzhou Medical University
Dianxin Zhou
Guangzhou Medical University
Zifeng Luo
Hunan Institute of Technology
Chao Zheng
Chinese Academy of Sciences
Xuhui Geng
Chinese Academy of Sciences
Zhenhao Liang
Huakeying Medical Technology (Guangzhou) Co., Ltd.
Song Wang
gzwangmomo1983@sina.com

Guangzhou Medical University

Research Article

Keywords: laser speckle contrast imaging, vascularity assessment, near-infrared autofluorescence, parathyroid gland, endoscopic surgery, thyroidectomy

Posted Date: June 29th, 2026

DOI: https://doi.org/10.21203/rs.3.rs-9942375/v1

License: This work is licensed under a Creative Commons Attribution 4.0 International License.
Read Full License

Additional Declarations: No competing interests reported.

Endoscopic NIRAF-LSCI Multimodal System with Pseudo-Color Visualization for Parathyroid Autofluorescence Localization and Tissue Perfusion Assessment: Preclinical Validation

Running title: Endoscopic LSCI for Parathyroid Function Prediction

Funding:
1.Ministry of Education Industry-University Cooperation Collaborative Education Project (No. 230902331264216);
2.Guangdong Provincial Education Science Planning Project (Higher Education Special Project （No. 2025GXJK0131);
3.Tertiary Education Scientific research project of Guangzhou Municipal Education Bureau (No. 2024312260)；
4.Clinical key specialty construction project funding of Guangdong Province （Guangdong Health Medical Letter [2023] No. 2）.
5.National College Students' Innovation and Entrepreneurship Training Program (Key Project), co-supported by Guangzhou Medical University Student Innovation Ability Enhancement Program (No. 01-451-2604-166)
Clinical trial number: not applicable.

ABSTRACT

Postoperative hypoparathyroidism remains a prevalent complication of thyroid surgery, primarily caused by unrecognized parathyroid gland (PG) injury or devascularization. While near-infrared autofluorescence (NIRAF) enables accurate PG localization, it provides no functional perfusion information; conversely, laser speckle contrast imaging (LSCI) offers label-free real-time perfusion assessment. Herein, we validated a multimodal endoscopic system integrating NIRAF and LSCI for simultaneous PG identification and vascular evaluation, focusing on LSCI perfusion performance and the clinical practicability of its pseudo-color semi-quantitative visualization. The system was tested in 8 Sprague–Dawley rats, where rat thyroids with homologous blood supply served as perfusion surrogates due to the minute volume of rat PGs. Imaging was performed under three strictly controlled in situ conditions: intact native vascularization, partial vascular occlusion, and complete vascular occlusion. LSCI pseudo-color visualization was generated via a standardized pipeline including temporal laser speckle contrast analysis (tLASCA)-based blood flow index (BFI) calculation, 5th–95th percentile normalization, and Jet colormap mapping. Intraoperative probe-based quantitative NIRAF was used for PG localization, and all results were validated against dual gold standards: intraoperative NIRAF probe detection and postoperative histopathology. NIRAF clearly identified PGs with a fluorescence intensity of 140.0±5.0 mV, significantly higher than thyroid (94.5±0.7 mV), trachea (83.0±4.0 mV), and muscle (52.0±2.0 mV) (all $P<0.001$), achieving 100% positive/negative predictive values and zero false results. LSCI speckle contrast increased progressively with decreasing perfusion, exhibiting a precise 1:1 correspondence with the continuous blue-to-red pseudo-color perfusion gradient, with histopathology confirming all fluorescent tissues as PGs. This multimodal system addresses two core clinical needs for intraoperative PG protection, and its standardized pseudo-color semi-quantitative workflow provides real-time label-free perfusion data with strong potential to guide clinical PG preservation decisions.

Keywords: laser speckle contrast imaging, vascularity assessment, near-infrared autofluorescence, parathyroid gland, endoscopic surgery, thyroidectomy

1 INTRODUCTION

Thyroid cancer has become the most common malignant neoplasm in the head and neck region, with a markedly increasing global incidence over the past three decades [1]. Surgery remains the first-line curative treatment for thyroid carcinoma. However, postoperative hypoparathyroidism persists as the most common complication, with reported incidence rates of 16% to 40% for transient hypoparathyroidism and 4% to 11% for permanent hypoparathyroidism after thyroidectomy. Permanent hypoparathyroidism necessitates lifelong supplementation of calcium and active vitamin D, severely impairing patients' quality of life and representing the leading cause of medical disputes in thyroid surgery. This complication mainly arises from inadvertent resection of the parathyroid glands (PGs) or unrecognized vascular injury during the operation [2].

Accurate intraoperative identification of PGs remains extremely challenging even for experienced surgeons, due to their minute volume, high variability in anatomical location, and gross appearance that is nearly indistinguishable from adjacent adipose tissue and lymph nodes [3]. Despite continuous advancements in surgical techniques, the rate of inadvertent parathyroidectomy during thyroid surgery remains as high as 13.2% [4]. Existing evidence-based medicine has confirmed that prophylactic autotransplantation of intraoperatively confirmed devascularized PGs can significantly improve graft survival and long-term functional recovery [2, 5]. Therefore, accurate intraoperative identification of PGs and reliable assessment of glandular perfusion status remain two core unmet clinical challenges in thyroid surgery.

Near-infrared autofluorescence (NIRAF) imaging leverages the unique endogenous fluorescence characteristics of PGs under 785 nm excitation and has demonstrated excellent detection sensitivity [6,7]. Devices based on this technology have been approved by the U.S. Food and Drug Administration (FDA) for intraoperative clinical use. A multicenter randomized controlled trial (RCT) by Benmiloud et al. [8] confirmed that NIRAF-assisted thyroid surgery significantly reduced the incidence of postoperative transient hypocalcemia, and a single-center RCT by Dip et al. [9] yielded consistent conclusions. Nevertheless, NIRAF only provides anatomical localization of PGs and offers no functional information regarding glandular perfusion—the key determinant of postoperative PG viability and function. This constitutes the limitation of its clinical application [10].

Indocyanine green (ICG) fluorescence imaging is widely applied for intraoperative parathyroid perfusion evaluation and aids in predicting postoperative parathyroid functional status [11]. However, it lacks real-time continuous blood flow monitoring capability and unified standardized semi-quantitative evaluation criteria; its fluorescence interpretation relies heavily on surgeons' subjective experience, leading to significant inter-observer variability. Additionally, it requires intravenous administration of exogenous contrast agents with potential allergic risks, accompanied by narrow imaging time windows and unavoidable in-vivo dye retention that easily causes diagnostic bias [12,13]. The latest meta-analysis by Jeong et al. [14] confirmed that although ICG angiography improves PG detection rate, these inherent limitations greatly restrict its routine clinical application.

Laser speckle contrast imaging (LSCI) is an emerging label-free microperfusion detection technology based on the principle of dynamic light scattering. It converts the motion state of red blood cells into speckle contrast values, which are inversely correlated with local blood flow velocity [15]. Compared with ICG, LSCI features no need for exogenous contrast agents, true real-time dynamic monitoring, and direct quantitative output of perfusion parameters [16]. Previous work by Cui et al. [17] first established a significant correlation between endoscopic LSCI-derived blood flow indices and early postoperative parathyroid hormone levels, confirming the clinical translational potential of LSCI for parathyroid function prediction. Nonetheless, their study only provided discrete quantitative blood flow values without enabling intraoperative real-time visual display and graded assessment of dynamic changes in PG microperfusion, requiring manual region-of-interest delineation and lacking intuitive perfusion gradient visualization for immediate surgical decision-making.

To fill this critical clinical and technical gap, we developed and preclinically validated a multimodal endoscopic system integrating NIRAF and LSCI. The primary objective of this study was to evaluate the efficacy of endoscopic LSCI for real-time PG perfusion assessment and the clinical practicability of its pseudo-color semi-quantitative visualization workflow. We aimed to demonstrate that endoscopic LSCI possesses sufficient detection sensitivity to differentiate well-perfused, ischemically impaired, and completely devascularized parathyroid-related tissues. By establishing a direct 1:1 causal correspondence between LSCI pseudo-color signals and true tissue perfusion status in real time, this system provides surgeons with immediate intraoperative feedback to guide decisions on PG in-situ preservation or prophylactic autotransplantation, eliminating the need to wait for postoperative hormonal results. We systematically evaluated the performance characteristics of this integrated strategy using a well-controlled rodent model.

2 MATERIALS AND METHODS

2.1 Experimental System and Main Instruments

The core instrument of this study was a self-developed multimodal fluorescence endoscopic system, jointly developed by our research team and Huakeying Medical Technology (Guangzhou) Co., Ltd. The system integrates two functional imaging modalities into a single endoscopic probe: a 785 nm-excited NIRAF imaging module for intraoperative localization and identification of PGs, and a 785 nm coherent light source LSCI module for real-time vascularity assessment. The detailed optical design of the system has been reported in our previous publication[18].

2.1.1 Endoscopic Laser Speckle Contrast Imaging System and Algorithms

The endoscopic laser speckle contrast imaging (eLSCI) module operates with a 785 nm laser source for coherent illumination, and acquires sequential raw speckle images under optimized exposure conditions to avoid saturation and ensure optimal speckle size matching with camera pixels. Raw image preprocessing includes dark-field correction, flat-field normalization, dead pixel removal, and region-of-interest (ROI) masking to eliminate interference from instruments and background noise.

The core perfusion quantification algorithm is Temporal Laser Speckle Contrast Analysis (tLASCA), whose basic imaging principles and algorithms have been detailed in our team's 2024 ASME publication [18]. For each pixel (x, y), speckle contrast $K_t(x,y)$ is calculated over a temporal window of M consecutive frames:

$$K_t(x,y) = \frac{\sqrt{\frac{1}{M}\sum_{m=1}^{M}[I(x,y,t_m)-\langle I(x,y)\rangle_T]^2}}{\langle I(x,y)\rangle_T}$$

Where $\langle I(x,y)\rangle_T$ denotes the temporal mean intensity, and $I(x,y,t_m)$ is the intensity at time t_m. Speckle contrast is inversely related to local blood flow: higher contrast indicates lower perfusion.

2.1.2 Blood Flow Index Calculation, Pseudocolor Transformation and Semi-quantitative Color Mapping

To convert contrast into a clinically intuitive perfusion metric, a Blood Flow Index (BFI) is computed:

$$\mathrm{BFI}(x,y)=\frac{1}{K(x,y)^2+\epsilon}$$

where ϵ is a small constant to avoid division by zero.

A critical improvement of this system is the pseudocolor mapping algorithm that converts grayscale perfusion maps into surgeon-friendly color-coded images. First, BFI values are normalized to the range [0, 1] using percentile clipping to suppress outliers:

$$P(x,y)=\frac{F(x,y)-F_{5\%}}{F_{95\%}-F_{5\%}}$$

where $F_{5\%}$ and $F_{95\%}$ represent the 5th and 95th percentiles of BFI in the ROI.

The normalized perfusion index $P(x,y)$ is then mapped to a Jet color map for real-time intraoperative display, where blue/purple corresponds to low perfusion (ischemic), green/yellow corresponds to moderate perfusion, and red/orange corresponds to high perfusion.

This mapping produces a continuous semi-quantitative color gradient that transitions smoothly and uninterruptedly from cool tones to warm tones, directly reflecting the progressive increase in tissue perfusion status from severe ischemia to optimal perfusion, without artificial discrete numerical grading. This intuitive continuous visualization enables rapid, objective intraoperative evaluation of parathyroid vascularity without the need for offline post-processing.

2.1.3 Motion Artifact Suppression and Multimodal Image Fusion

To improve stability in endoscopic conditions, a temporal autocorrelation decorrelation algorithm is applied to reduce artifacts from respiration and surgical manipulation. Multimodal images (white-light, NIRAF, and pseudocolor perfusion) are spatially aligned and fused, allowing simultaneous identification and functional assessment of parathyroid glands in a single view.

2.2 Probe-Based NIRAF Detector for Quantitative Validation

A high-sensitivity near-infrared laser-induced fluorescence detector (Dalian Institute of Chemical Physics, Chinese Academy of Sciences, China) was used for quantitative validation of NIRAF imaging results. This probe-based device employed a 785 nm excitation wavelength and displayed real-time fluorescence intensity in millivolts (mV). An audible feedback was triggered when the detected value reached 100 mV to indicate suspected PG tissue. The intraoperative verification system and positive judgment criteria of this probe-based NIRAF technology have been established and clinically validated in the classic study by Duan et al. [19].

2.3 Experimental Animals and Ethical Approval

All animal experiments were approved by the Institutional Animal Care and Use Committee (IACUC) of Guangzhou Medical University (ethical approval number: S2024-080, approval date: July 23, 2024) and performed in strict accordance with relevant regulations for laboratory animal care and use. Eight healthy Sprague–Dawley (SD) rats (4 male, 4 female), weighing 200–500 g and aged 6–13 weeks, were provided by Zhuhai Baishitong Biotechnology Co., Ltd. Animals were

housed in a standard laboratory environment with free access to food and water and acclimatized for 1 week before experiments.

2.4 Experimental Methods

2.4.1 Surgical Procedure and Tissue Harvesting

Rats were anesthetized via intraperitoneal injection of 10% chloral hydrate at a dose of 0.3 mL/100 g, with anesthesia confirmed by loss of the righting reflex and absence of the pedal withdrawal reflex. Rats were then fixed in the supine position on the operating board, and a sterile gauze pad was placed under the neck to fully expose the surgical field. A midline longitudinal incision of approximately 2.0–2.5 cm was made in the neck, followed by sequential incision of the skin and subcutaneous tissue. The sternohyoid muscles anterior to the trachea were bluntly dissected to fully expose the trachea, thyroid cartilage, and bilateral thyroid glands.

After adequate exposure of the surgical field, three strictly controlled in situ perfusion conditions were established sequentially for LSCI perfusion assessment. First, baseline imaging was performed under native vascularization, where the thyroid gland was fully exposed without any vascular injury, and the superior thyroid vessels, inferior thyroid vessels, and thyroid isthmus remained completely intact. Partial vascular occlusion was then induced by transecting the thyroid isthmus and ligating either the unilateral superior or inferior thyroid vessels with 4-0 silk sutures, preserving approximately one-third to one-half of the native blood supply. Finally, complete vascular occlusion was achieved by transecting the thyroid isthmus and ligating all major vascular pedicles, including bilateral superior thyroid vessels, inferior thyroid vessels, and lateral thyroid vessels, resulting in more than 90% loss of glandular blood perfusion.

In situ multimodal imaging, including NIRAF localization and LSCI perfusion assessment, was performed sequentially under each of the above perfusion conditions. Subsequently, bilateral thyroid glands, parathyroid glands, trachea, esophagus, muscle, fat, and other related cervical tissues were carefully bluntly dissected and en bloc harvested for ex vivo validation experiments. The excised tissue blocks were immediately placed on sterile gauze moistened with normal saline to maintain tissue viability during subsequent ex vivo imaging procedures.

2.4.2 NIRAF Imaging and Probe Quantitative Validation

The multimodal fluorescence endoscope was switched to NIRAF mode with 785 nm excitation. Ambient light was turned off to minimize stray light interference. The excised tissue blocks were placed under the endoscopic field of view, and full-field scanning imaging was performed on the ventral and dorsal sides of the thyroid, anatomical regions of the parathyroid glands, trachea, esophagus, and muscle tissue respectively, with fluorescence images recorded. The number of parathyroid glands detected by the NIRAF visual mode was counted for each rat individually, and the correlation between the detection rate and the age, body weight and developmental status of the rats was analyzed.

The probe-based NIRAF detector was used for quantitative validation of suspected parathyroid regions identified by NIRAF mode and control tissues, including thyroid, trachea and muscle. The probe tip was gently applied to the tissue surface, and the fluorescence intensity displayed on the software interface was recorded. For rats with no specific fluorescence signal detected by NIRAF mode, full-area point-by-point scanning was performed on all isolated cervical tissues with the probe-based NIRAF detector, and the fluorescence detection results were recorded.

2.4.3 Pathological Gold Standard Validation

All tissue samples were fixed in 4% paraformaldehyde for 24 hours, then routinely embedded in paraffin, serially sectioned at 4 μm thickness, and stained with hematoxylin-eosin (HE). Histological analysis was performed by a pathologist blinded to the fluorescence imaging results to confirm the tissue type, and verify the consistency between NIRAF imaging results, probe detection results and the pathological gold standard.

2.4.4 LSCI Perfusion Imaging Experiment

Limited by the anatomical characteristics of SD rat parathyroid glands, the rat thyroid gland was used as a surrogate model for parathyroid perfusion assessment in this study. The two tissues are anatomically adjacent with a homologous blood supply pattern[16], and the volume and weight of the rat thyroid gland have a higher matching degree with human parathyroid glands, which can meet the imaging requirements of LSCI microcirculation perfusion assessment. The comparison of anatomical and morphological parameters among SD rat thyroid, SD rat parathyroid gland, and normal human parathyroid gland is shown in Table 1.

Table 1 Comparison of anatomical and morphological parameters among SD rat thyroid, SD rat parathyroid gland, and normal human parathyroid gland

Parameter Dimension	SD Rat Thyroid	SD Rat Parathyroid Gland	Normal Human Parathyroid Gland
Morphological Structure	Bilateral lobes connected by isthmus, attached to both sides of trachea	Usually 2 pairs of 4 glands with number variation	Usually 4 glands (1 superior and 1 inferior pair), 5%-15% of population have supernumerary glands
Core Size	Unilateral lobe: 3-5 mm length, 2-3 mm width, 1-2 mm thickness	Single gland diameter 0.3-0.5 mm, volume 0.5-1 mm^3	Single gland: 3-8 mm length, 2-4 mm width, 0.5-2 mm thickness
Weight	Total weight 10-20 mg	0.2-0.5 mg per gland	30-50 mg per gland, total weight 120-200 mg
Anatomical Location	Ventral side of trachea, immediately below thyroid cartilage	Superior glands: dorsal side of upper thyroid pole or near thymus; inferior glands: near lower thyroid pole or within thymus	Superior glands: mostly at cricoid cartilage level behind upper thyroid pole; inferior glands: near lower thyroid pole, may be ectopic to thymus or mediastinum
Imaging Adaptability	Sufficient volume for full-field microcirculation imaging with LSCI	Extremely small volume with large anatomical variation, unable to achieve stable LSCI perfusion imaging	Target tissue for intraoperative LSCI imaging in clinical practice, high volume matching with rat thyroid

The LSCI module was connected to the endoscopic system, and imaging was performed on thyroid glands under three different perfusion conditions, namely intact native vascularization,

partial vascular occlusion, and complete vascular occlusion.According to the LSCI imaging and pseudo-color conversion workflow established in section 2.1, speckle image acquisition, preprocessing, contrast calculation, pseudo-color mapping and semi-quantitative analysis were completed under different perfusion states. The differences in speckle contrast and pseudo-color perfusion grading under different perfusion states were qualitatively compared to evaluate the sensitivity of LSCI to dynamic changes in tissue perfusion.The 1:1 correspondence between raw black-and-white speckle images and pseudo-color perfusion maps was verified, with the raw black-and-white speckle results as the gold standard for LSCI perfusion assessment.

2.5 Statistical Analysis

Data analysis was performed using SPSS 26.0 software. Fluorescence intensity measured by the probe-based detector was expressed as mean ± standard deviation (SD). Independent-samples t-tests were used to compare fluorescence intensity between suspected parathyroid glands and control tissues (thyroid, trachea, muscle).Diagnostic efficacy indicators including PPV, NPV, false positive rate and false negative rate were calculated with histopathological results as the gold standard. A two-sided α level of 0.05 was used, and $P < 0.05$ was considered statistically significant.

3 RESULTS

3.1 Identification Efficacy of Parathyroid Glands by Multimodal Endoscopic NIRAF Mode

3.1.1 Detection Rate of Parathyroid Glands by NIRAF Visual Method

The age, body weight and number of parathyroid glands detected by NIRAF visual mode of the 8 SD rats are shown in Table 2. A total of 5 specific high-fluorescence signal foci were identified on the dorsal aspect of the thyroid gland in 4 out of 8 rats using the multimodal endoscopic NIRAF visual mode. The overall detection rate of PGs at the individual rat level was 50%.

Table 2 Statistics of the number of parathyroid glands detected by NIRAF mode in different rats

Rat Number	Age (week)	Body Weight (g)	Number of PGs Detected by NIRAF Mode
1	6	200	0
2	6	200	0
3	6	200	0
4	6	300	1
5	10	450	1
6	10	450	0
7	13	500	1
8	13	500	2
Total	-	-	5

Combined with the data in Table 2 and pathological results, the core reasons for the limited detection rate were directly related to the developmental status and anatomical characteristics of

rat parathyroid glands. The first influencing factor was the extremely small volume of rat parathyroid glands. The developmental degree of the glands was positively correlated with age and body weight. The gland development in 6-week-old rats weighing 200 g was low, which exceeded the effective resolution threshold of endoscopic fluorescence imaging. No glands were detected in 3 rats weighing 200 g at this age, and only 1 gland was detected in 1 rat weighing 300 g. The second influencing factor was the ectopic anatomical location of parathyroid glands. Some glands were located outside the conventional cervical surgical field such as the thymus, which could not be covered by the endoscopic field of view. The third influencing factor was that some glands were completely embedded in the thyroid parenchyma. The 785 nm near-infrared excitation light could not penetrate the thyroid tissue for effective detection, thus failing to capture specific autofluorescence signals.

3.1.2 Quantitative Comparison of Fluorescence Intensity Between PGs and Surrounding Tissues

Quantitative detection results of the probe-based NIRAF detector showed that the fluorescence intensity of pathologically confirmed PG tissue was 140.0 ± 5.0 mV, which was significantly higher than that of surrounding control tissues. The fluorescence intensity of thyroid tissue was 94.5 ± 0.7 mV, with $t=18.23$ and $P < 0.001$ for intergroup comparison. The fluorescence intensity of tracheal tissue was 83.0 ± 4.0 mV, with $t=12.45$ and $P < 0.001$ for intergroup comparison. The fluorescence intensity of muscle tissue was 52.0 ± 2.0 mV, with $t=36.50$ and $P < 0.001$ for intergroup comparison. The specific data are shown in Table 3. These results further confirmed the high specific recognition ability of 785 nm-excited NIRAF technology for PG tissue, which was consistent with the autofluorescence characteristics of PGs reported in previous studies. Representative multimodal imaging results and pathological validation of PG identification are presented in Fig. 1.

Table 3 Fluorescence intensity of different rat tissues measured by the probe-based NIRAF detector

Tissue Type	Fluorescence Intensity (mV)	t-value (vs. PG)	P-value (vs. PG)
Suspected Parathyroid (PG)	140.0 ± 5.0	—	—
Thyroid	94.5 ± 0.7	18.23	< 0.001
Trachea	83.0 ± 4.0	12.45	< 0.001
Muscle	52.0 ± 2.0	36.50	< 0.001

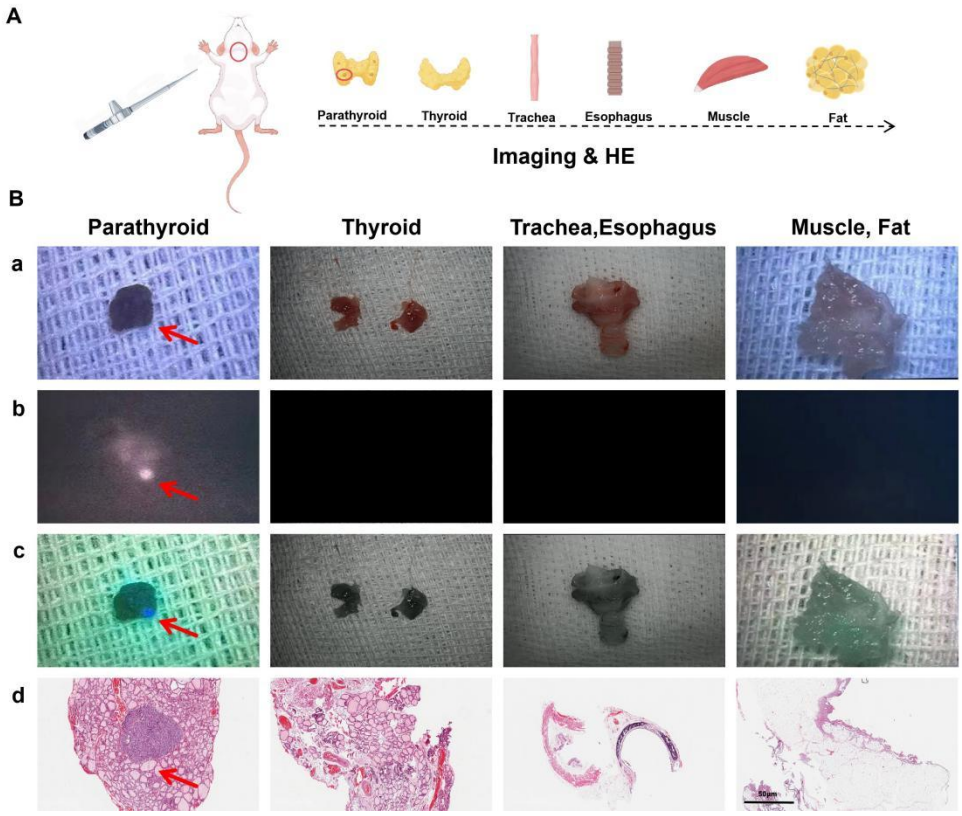


Fig 1 Specific identification of parathyroid glands using near-infrared autofluorescence (NIRAF) imaging with pathological validation.

(A) Schematic of the experimental workflow. Cervical tissues from SD rats, including parathyroid, thyroid, esophagus, trachea, muscle and fat, were imaged using the integrated NIRAF-LSCI endoscopic system, followed by hematoxylin-eosin (HE) staining for pathological confirmation (B) Representative multimodal imaging and pathological results. Rows: (a) endoscopic white light mode; (b) endoscopic fluorescence mode; (c) endoscopic fusion light mode; (d) HE staining. Red arrows indicate parathyroid glands. Only parathyroid tissue showed specific strong NIRAF signal, while thyroid, trachea, esophagus, muscle and fat exhibited no obvious fluorescence. Pathological results confirmed the identity of all fluorescent tissues as parathyroid glands

3.1.3 Consistency Validation Between Visual, Probe and Pathological Results

For the 5 high-fluorescence signal foci identified by the NIRAF visual method, secondary quantitative validation was performed using the probe-based NIRAF detector. The results showed that the fluorescence intensity of all 5 foci reached the positive judgment threshold of 100 mV, and the detector triggered specific audible feedback for all foci. These results were fully consistent with the identification results of the visual method. Postoperative pathological examination confirmed that all 5 high-fluorescence signal foci were PG tissue, with no non-PG tissues such as thyroid, lymph nodes, fat, or trachea misjudged.

For the 4 rats with no specific fluorescence signal detected by the NIRAF visual method, namely No.1, No.2, No.3 and No.6, full-area point-by-point scanning was performed on all isolated cervical tissues using the probe-based NIRAF detector. The detection scope included thyroid, trachea, esophagus, muscle, fat and thymus. The results showed that no specific fluorescence signal reaching the 100 mV threshold was detected in any tissues. These results were completely consistent with the negative judgment of the visual method. Postoperative histopathological examination confirmed that no PG structure was found in all submitted tissues

of the 4 rats, which was consistent with the negative results of the visual method and probe method.

The diagnostic efficacy indicators of NIRAF visual mode for PG identification are summarized in Table 4, with the probe-based quantitative detection and histopathological results as the double gold standard.

Table 4 Diagnostic efficacy of NIRAF visual mode for rat PG identification

Diagnostic Efficacy Index	Value
Individual rat detection rate	50% (4/8)
Positive Predictive Value (PPV)	100% (5/5)
Negative Predictive Value (NPV)	100% (4/4)
False Positive Rate	0% (0/5)
False Negative Rate	0% (0/4)

3.2 Dynamic Assessment Efficacy of Tissue Perfusion by Multimodal Endoscopic LSCI Mode

3.2.1 Variation Pattern of Speckle Contrast Under Different Perfusion Conditions

LSCI imaging results showed that this technology had extremely high sensitivity to dynamic changes in tissue blood flow. Tissue perfusion level was significantly negatively correlated with laser speckle contrast. With the stepwise decrease of tissue perfusion level, the speckle contrast increased progressively. The in situ thyroid tissue with intact perfusion had the most abundant blood flow, the highest dynamic decorrelation degree of the speckle pattern, and presented the lowest speckle contrast. After ligation of the superior and inferior thyroid arteries to induce ischemia, the blood perfusion in the thyroid tissue decreased significantly, the stability of the speckle pattern was significantly improved, and the speckle contrast was significantly higher than that in the intact perfusion state. The completely resected ex vivo devascularized thyroid tissue had no dynamic blood flow signal, the speckle pattern was completely stable, and presented the highest speckle contrast. The above results confirmed that the endoscopic LSCI mode can effectively distinguish well-perfused, ischemically compromised, and completely devascularized tissues, and speckle contrast can be used as a reliable surrogate marker for tissue perfusion status, which was consistent with the blood flow detection principle of LSCI technology reported in previous studies. The raw black-and-white speckle images were used as the qualitative gold standard for LSCI perfusion assessment in this study (Fig 2).

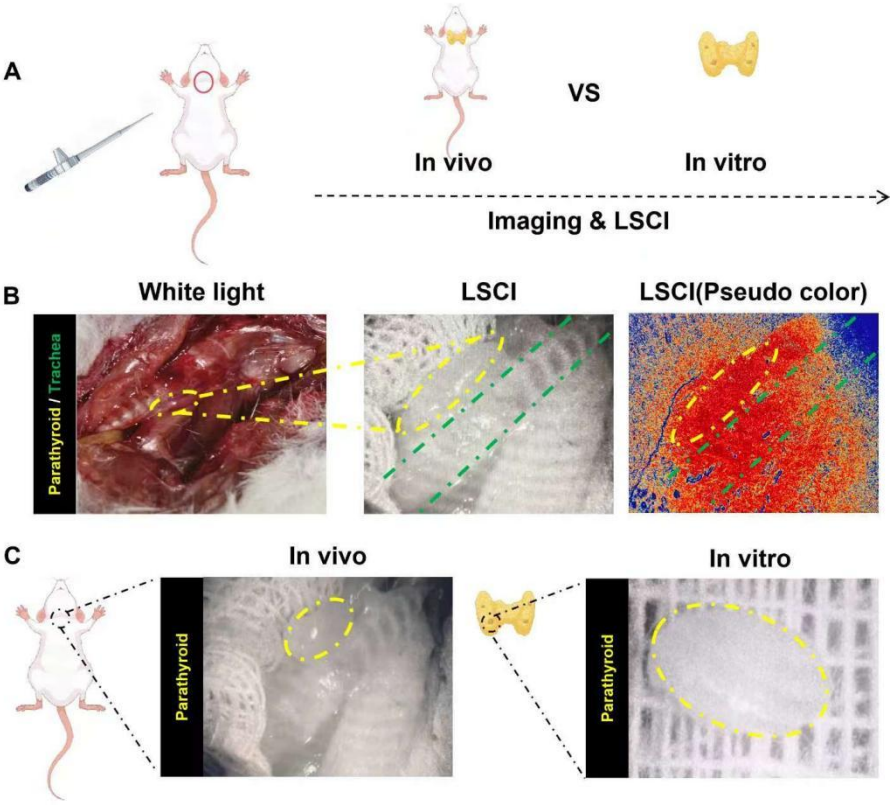


Fig 2 In vivo and ex vivo multimodal imaging of rat parathyroid glands using the integrated NIRAF-LSCI system.

(A) Schematic of the experimental workflow. In vivo imaging was performed on anesthetized SD rats using the integrated system combining NIRAF, LSCI and pseudo-color semi-quantitative mapping, followed by ex vivo validation of harvested parathyroid glands.

(B) Representative intraoperative images: white light, raw laser speckle contrast imaging (LSCI), and pseudo-color-coded LSCI perfusion map. Yellow dashed lines mark the parathyroid gland; green dashed lines mark the trachea. The pseudo-color map shows high perfusion (red signal) in the parathyroid and adjacent thyroid tissue.

(C) Comparison of raw LSCI images of parathyroid glands in vivo (left) and ex vivo (right). Yellow dashed circles indicate the parathyroid glands.

3.2.2 Pseudo-color Semi-quantitative Imaging Results

Based on the whole workflow of LSCI imaging and pseudo-color transformation established in the method section, the conversion from original black-and-white speckle images to clinically readable pseudo-color perfusion maps was completed in this study, realizing real-time visualization and semi-quantitative analysis of intraoperative tissue perfusion status. In the original black-and-white speckle images, the intact perfusion area with low contrast corresponded to high perfusion index after transformation, and presented high perfusion performance in red in the pseudo-color map. The ex vivo ischemic area with high contrast corresponded to low perfusion index after transformation, and presented no perfusion performance in blue in the pseudo-color map. The partially ischemic area with moderate perfusion corresponded to medium perfusion index after transformation, and presented orange-yellow performance in the pseudo-color map.

The contrast features of raw speckle images corresponded well to the pseudo-color perfusion

presentation, and the transformed color distribution was highly consistent with real tissue perfusion status. Different perfusion levels could be intuitively distinguished by a continuously transitioning color scale, which achieved a smooth gradient display from low perfusion to high perfusion without artificial discrete numerical grading. Compared with conventional grayscale speckle imaging, this pseudo-color visualization mode enables real-time intraoperative interpretation, possesses strong anti-interference capability and favorable imaging stability for clinical application (Fig.3).

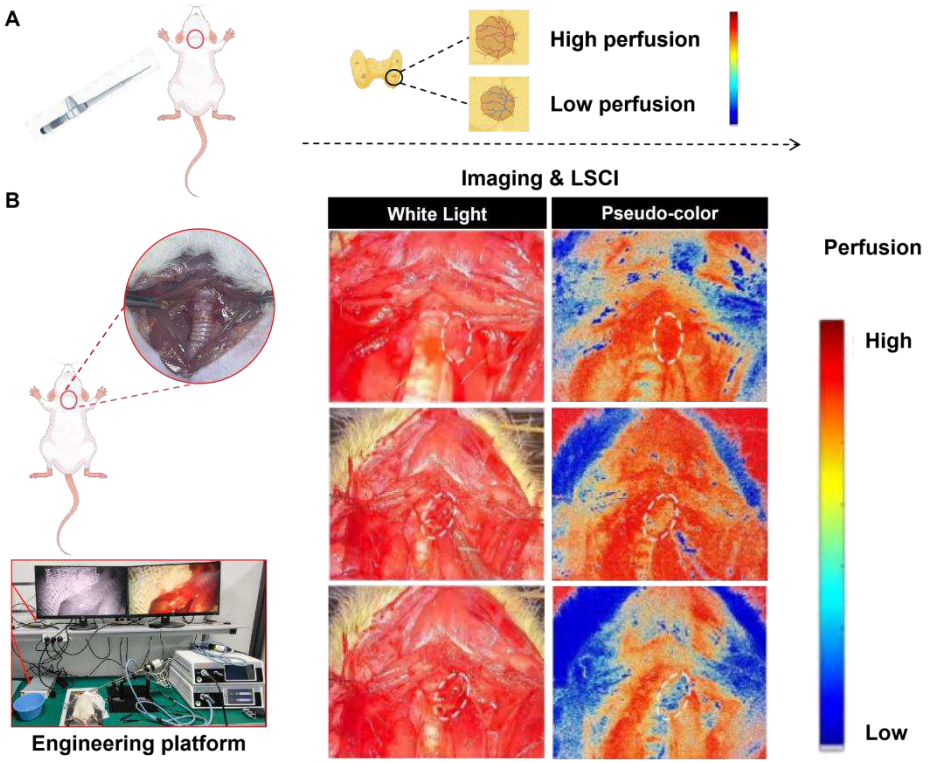


Fig 3 Semi-quantitative in vivo tissue perfusion assessment based on the integrated NIRAF-LSCI endoscopic system.

(A) Schematic of experimental design and continuous perfusion gradient. Anesthetized SD rats were imaged with the integrated endoscopic system combining near-infrared autofluorescence (NIRAF), laser speckle contrast imaging (LSCI), and pseudo-color semi-quantitative mapping. The color bar presents a smooth continuous transition from cool tones to warm tones, in which the gradual color increment corresponds to a progressive increase in tissue perfusion from ischemia to well-perfused status.

(B) Representative intraoperative results. Left: custom-built multimodal endoscopic platform. Right: three paired white-light and pseudo-color LSCI maps, corresponding to three vascular states (top to bottom): intact perfusion, partial vascular occlusion, and complete transection. White dashed circles mark parathyroid glands, showing the continuous transition from red (high perfusion) to blue (low perfusion) with progressive vascular injury.

4 DISCUSSION

The integrated NIRAF-LSCI multimodal endoscopic system developed in this study directly addresses the two core unmet clinical needs in thyroid surgery: accurate intraoperative PG identification and real-time vascular viability assessment. This preclinical study systematically validated the performance of our integrated system and experimentally verified two technical conclusions: 785 nm-excited NIRAF enables highly specific PG identification, and endoscopic

LSCI can quantitatively capture perfusion gradients and visualize raw data via a standardized pseudo-color mapping workflow.

The NIRAF module exhibited excellent specific identification performance. The 50% overall PG detection rate in rats was not due to technical limitations of our system, but exclusively to the inherent anatomical and developmental characteristics of rodent PGs, which inherently impose far greater detection challenges than human clinical scenarios. Rat PGs showed a fluorescence intensity of 140.0±5.0 mV, significantly higher than rat thyroid (94.5±0.7 mV), rat trachea (83.0±4.0 mV) and rat muscle (52.0±2.0 mV) (all $P<0.001$). Consistent with Cousart et al. [20], parathyroid tissue possesses inherently stronger autofluorescence than surrounding neck soft tissues. Using intraoperative probe NIRAF and postoperative histopathology as dual gold standards, NIRAF visual mode achieved 100% PPV/NPV with zero false results. The limited detection rate was explained by three interrelated factors: underdeveloped glands in young rats, ectopic locations outside the cervical surgical field (including intrathyroidal embedding and thymic localization), and intrathyroidal glands blocking 785 nm excitation—all well-recognized causes of missed detection in clinical practice [20]. Notably, the fact that our system maintained perfect diagnostic accuracy (100% PPV/NPV) despite the elevated detection difficulty of the rat model provides strong evidence for the high reliability and superior performance of our NIRAF imaging module.

The endoscopic LSCI module exhibited high sensitivity to real-time dynamic changes in tissue microperfusion. Under three strictly controlled perfusion states (intact vascularization, partial occlusion, complete devascularization), LSCI speckle contrast increased progressively with decreasing perfusion, showing a stable linear negative correlation. By eliminating confounding factors inherent to clinical surgery, this study established a strict quantitative causal relationship between LSCI speckle signals and perfusion levels, whereas clinical ICG studies can only perform correlation analysis due to individual variability and intraoperative confounders. While LSCI perfusion patterns align with the principles of ICG angiography [21,22], conventional ICG evaluation relies heavily on subjective visual scoring, lacks continuous semi-quantitative output, and inevitably interferes with NIRAF signal acquisition [21,22]. In contrast, our label-free LSCI enables synchronous multimodal fusion without signal interference. Furthermore, the exact 1:1 correspondence between raw speckle images and standardized pseudo-color perfusion maps validates the stability, reproducibility and diagnostic accuracy of our workflow.

To achieve accurate imaging of the fine parathyroid microcirculation, we selected temporal laser speckle contrast analysis (tLASCA) as the core algorithm. Unlike spatial LSCI (sLSCI), which causes spatial resolution loss via 7×7 sliding window averaging incompatible with tiny PGs, tLASCA also exhibits inherent resistance to static scattering from surgical instruments, eliminating complex intraoperative calibration [15].

Building on the tLASCA framework, we developed an optimized version for miniaturized endoscopic platforms. Existing advanced LSCI techniques, including principal component analysis-based depth correction [23] and single-exposure calibration [24], suffer from high computational latency and require laborious pre-procedural calibration. Optical flow-based approaches offer enhanced resolution but lack validated quantitative accuracy and real-time capability [25]. In contrast, our optimized tLASCA enables true real-time imaging at 39 frames per second. Standardized 5th–95th percentile normalization suppresses artifacts from laser intensity fluctuations and variable imaging distances, while temporal autocorrelation-based motion

correction enhances stability during endoscopic manipulation.

The most prominent innovation of this system is our standardized continuous pseudo-color semi-quantitative mapping framework, which delivers two layered technical advantages over existing methods. First, it addresses the fundamental limitation of conventional grayscale speckle maps: unlike traditional grayscale outputs that require time-consuming offline post-processing and specialized technical interpretation, our system converts raw speckle data into surgeon-friendly color-coded images in real time via 5th–95th percentile normalization and Jet colormap mapping, transforming abstract contrast values into an intuitive smooth blue-to-red gradient that directly reflects tissue perfusion status. Second, it overcomes the critical defects of existing pseudo-color strategies: this continuous scheme avoids artificial discrete numerical grading and effectively suppresses interference from environmental variables such as laser intensity fluctuations and imaging distance variations. In contrast, Miller et al. [26] used only a single green color to highlight vascular structures without distinguishing differential perfusion levels, while Heeman et al.[27] implemented a three-grade discrete mapping that cannot accurately quantify microperfusion heterogeneity. Collectively, these two complementary advantages establish a direct, real-time link between objective LSCI perfusion signals and intraoperative surgical decision-making.

Broader clinical translation of endoscopic LSCI for parathyroid protection faces three core barriers: high-resolution miniaturized probes, robust motion artifact suppression, and seamless multimodal integration. Our team previously addressed the first two with a unified 785 nm laser source prototype integrating NIRAF and LSCI via real-time co-registration [18]. This study completes the technical framework by adding the standardized continuous pseudo-color semi-quantitative workflow, addressing all three translational barriers.

LSCI is widely used in neurosurgery [28], renal [29] and gastrointestinal surgery [30], but few systems are optimized for parathyroid anatomy. Current dedicated platforms have critical limitations: the open-surgery-only ParaSPAI system has dual-path registration errors and provides only grayscale images [16,31], while Cui et al.'s endoscopic system is single-modality and requires manual ROI delineation [17]. Our single-probe multimodal design eliminates registration errors and enables simultaneous real-time PG localization and perfusion assessment.

There are still three objective limitations in this study that need to be gradually improved in subsequent research. First, small-sample rodent experiments limit clinical extrapolation, requiring future validation in large animal models. Second, rat thyroid tissue was used as a perfusion surrogate due to tiny PG size, necessitating direct validation on human PGs. Third, this preclinical validation did not include parathyroid hormone endpoints, requiring prospective clinical trials to establish correlations between LSCI parameters and long-term gland function.

In conclusion, this preclinical study validated that the integrated NIRAF-LSCI multimodal endoscopic system enables highly specific PG identification and label-free real-time tissue perfusion assessment. Endoscopic LSCI exhibits high sensitivity to dynamic perfusion changes, and the standardized continuous pseudo-color semi-quantitative transformation method demonstrates favorable intraoperative applicability. This work complements the methodological framework for endoscopic LSCI in parathyroid protection, lays a solid foundation for clinical translation, and is expected to reduce the risk of postoperative hypoparathyroidism.

5 CONCLUSIONS

This preclinical study validates our integrated NIRAF-LSCI multimodal endoscopic system for highly specific parathyroid identification and real-time label-free perfusion assessment. The

unified 785 nm laser source design enables seamless anatomical-functional integration, while the standardized continuous pseudo-color workflow provides objective perfusion data to guide intraoperative parathyroid preservation decisions. This system holds strong clinical translation potential to reduce postoperative hypoparathyroidism in minimally invasive thyroid surgery.

Abbreviations

BFI	Blood Flow Index
FDA	U.S. Food and Drug Administration
HE	Hematoxylin-Eosin
ICG	Indocyanine Green
LSCI	Laser Speckle Contrast Imaging
NIRAF	Near-Infrared Autofluorescence
NPV	Negative Predictive Value
ParaSPAI	Parathyroid Speckle and Autofluorescence Imager
PGs	Parathyroid Glands
PPV	Positive Predictive Value
PTH	Parathyroid Hormone
RCT	Randomized Controlled Trial
ROI	Region of Interest
SD	Sprague-Dawley
sLSCI	Spatial Laser Speckle Contrast Imaging
tLASCA	Temporal Laser Speckle Contrast Analysis
tLSCI	Temporal Laser Speckle Contrast Imaging

REFERENCES

[1] Sung H, Ferlay J, Siegel RL, et al. Global Cancer Statistics 2020: GLOBOCAN Estimates of Incidence and Mortality Worldwide for 36 Cancers in 185 Countries. CA Cancer J Clin. 2021;71(3):209-249. https://doi.org/10.3322/caac.21660

[2] Zhu J, Tian W, Xu Z, et al. Expert consensus statement on parathyroid protection in thyroidectomy. Ann Transl Med. 2015;3(16):230. https://doi.org/10.3978/j.issn.2305-5839.2015.08.20

[3] Lappas D, Noussios G, Anagnostis P, et al. Location, number and morphology of parathyroid glands: results from a large anatomical series. Anat Sci Int. 2012;87(3):160-164. https://doi.org/10.1007/s12565-012-0142-1

[4] Asya O, Yumuşakhuylu AC, Gündoğdu Y, et al. Thyroid Surgery and Inadvertent Removal of Parathyroids. Indian J Otolaryngol Head Neck Surg. 2022;74(Suppl 3):6022-6026. https://doi.org/10.1007/s12070-021-02590-0

[5] Hicks G, George R, Sywak M. Short and long-term impact of parathyroid autotransplantation on parathyroid function after total thyroidectomy. Gland Surg. 2017;6(Suppl 1):S75-S85. https://doi.org/10.21037/gs.2017.09.15

[6] Paras C, Keller M, White L, et al. Near-infrared autofluorescence for the detection of parathyroid glands. J Biomed Opt. 2011;16(6):067012. https://doi.org/10.1117/1.3583571

[7] Wang B, Zhu CR, Liu H, et al. The Accuracy of Near Infrared Autofluorescence in Identifying Parathyroid Gland During Thyroid and Parathyroid Surgery: A Meta-Analysis. Front Endocrinol

(Lausanne). 2021;12:701253. https://doi.org/10.3389/fendo.2021.701253
[8] Benmiloud F, Godiris-Petit G, Gras R, et al. Association of Autofluorescence-Based Detection of the Parathyroid Glands During Total Thyroidectomy With Postoperative Hypocalcemia Risk: Results of the PARAFLUO Multicenter Randomized Clinical Trial. JAMA Surg. 2020;155(2):106-112. https://doi.org/10.1001/jamasurg.2019.4613
[9] Dip F, Falco J, Verna S, et al. Randomized Controlled Trial Comparing White Light with Near-Infrared Autofluorescence for Parathyroid Gland Identification During Total Thyroidectomy. J Am Coll Surg. 2019;228(5):744-751. https://doi.org/10.1016/j.jamcollsurg.2018.12.044
[10] Solórzano CC, Thomas G, Berber E, et al. Current state of intraoperative use of near infrared fluorescence for parathyroid identification and preservation. Surgery. 2021;169(4):868-878. https://doi.org/10.1016/j.surg.2020.09.014
[11] Lavazza M, Liu X, Wu C, et al. Indocyanine green-enhanced fluorescence for assessing parathyroid perfusion during thyroidectomy. Gland Surg. 2016;5(5):512-521. https://doi.org/10.21037/gs.2016.10.06
[12] Mannoh EA, Baregamian N, Thomas G, et al. Comparing laser speckle contrast imaging and indocyanine green angiography for assessment of parathyroid perfusion. Sci Rep. 2023;13(1):17270. https://doi.org/10.1038/s41598-023-42649-2
[13] Ladurner R, Sommerey S, Arabi NA, et al. Intraoperative near-infrared autofluorescence imaging of parathyroid glands. Surg Endosc. 2017;31(8):3140-3145. https://doi.org/10.1007/s00464-016-5338-3
[14] Nguyen VC, Song CM, Ji YB, et al. Efficacy and role of indocyanine green angiography in thyroidectomy: a systematic review and meta-analysis. Eur Arch Otorhinolaryngol. 2025;282(10):4935-4947. https://doi.org/10.1007/s00405-025-09370-4
[15] Boas DA, Dunn AK. Laser speckle contrast imaging in biomedical optics. J Biomed Opt. 2010;15(1):011109. https://doi.org/10.1117/1.3285504
[16] Mannoh EA, Thomas G, Solórzano CC, et al. Intraoperative Assessment of Parathyroid Viability using Laser Speckle Contrast Imaging. Sci Rep. 2017;7(1):14798. https://doi.org/10.1038/s41598-017-14941-5
[17] Cui Y, Zou M, Song B, et al. Endoscopic laser speckle imaging enables real-time prediction of parathyroid function in thyroidectomy. Lasers Med Sci. 2025;40(1):508. https://doi.org/10.1007/s10103-025-04760-w
[18] Wen Q, Cai C, Fang J, et al. A Miniaturized Endoscopic Device Integrating Raman Spectroscopy and Laser Speckle Technology Via an Image Fusion Algorithm for Intraoperative Identification and Functional Protection of Parathyroid Glands. J Med Devices. 2024;18(2):021004. https://doi.org/10.1115/1.4065481
[19] Duan Y, Wang C, Geng X, et al. A highly sensitive optical fiber based near-infrared laser induced fluorescence detector (LIF) for parathyroid gland detection. Sens Actuators B Chem. 2022;364:131879. https://doi.org/10.1016/j.snb.2022.131879
[20]Cousart AG, Kiernan CM, Willmon PA, et al. Near-Infrared Autofluorescence for Parathyroid Detection During Endocrine Neck Surgery: A Randomized Clinical Trial. JAMA Surg. 2025;160(9):936-944. https://doi.org/10.1001/jamasurg.2025.2233
[21] Yin S, Pan B, Yang Z, et al. Combined Use of Autofluorescence and Indocyanine Green Fluorescence Imaging in the Identification and Evaluation of Parathyroid Glands During Total Thyroidectomy: A Randomized Controlled Trial. Front Endocrinol (Lausanne). 2022;13:897797.

https://doi.org/10.3389/fendo.2022.897797
[22] Di Lorenzo S, Carrillo Lizarazo JL, Dionigi G, et al. Impact of near-infrared fluorescence imaging plus indocyanine green fluorescence on postoperative hypoparathyroidism rates after total thyroidectomy and central neck lymph node dissection. Br J Surg. 2024;111(2):znae022. https://doi.org/10.1093/bjs/znae022
[23] Surkov Y, Timoshina P, Serebryakova I, et al. Laser speckle contrast imaging with principal component and entropy analysis: a novel approach for depth-independent blood flow assessment. Front Optoelectron. 2025;18(1):1. https://doi.org/10.1007/s12200-024-00143-1
[24] Wang C, Cao Z, Jin X, et al. Robust quantitative single-exposure laser speckle imaging with true flow speckle contrast in the temporal and spatial domains. Biomed Opt Express. 2019;10(8):4097-4114. https://doi.org/10.1364/BOE.10.004097
[25] Aminfar A, Davoodzadeh N, Aguilar G, et al. Application of optical flow algorithms to laser speckle imaging. Microvasc Res. 2019;122:52-59. https://doi.org/10.1016/j.mvr.2018.11.001
[26] Miller DR, Ashour R, Sullender CT, et al. Continuous blood flow visualization with laser speckle contrast imaging during neurovascular surgery. Neurophotonics. 2022;9(2):021908. https://doi.org/10.1117/1.NPh.9.2.021908
[27] Heeman W, Maassen H, Calon J, et al. Real-time visualization of renal microperfusion using laser speckle contrast imaging. J Biomed Opt. 2021;26(5):056004. https://doi.org/10.1117/1.JBO.26.5.056004
[28] Hecht N, Woitzik J, König S, et al. Laser speckle imaging allows real-time intraoperative blood flow assessment during neurosurgical procedures. J Cereb Blood Flow Metab. 2013;33(7):1000-1007. https://doi.org/10.1038/jcbfm.2013.42
[29] Noël J, Mascarenhas A, Nwaiwu CA, et al. Laser speckle contrast imaging compared with indocyanine green in renal perfusion of a porcine model. Curr Urol. 2023;17(2):141-145. https://doi.org/10.1097/CU9.0000000000000155
[30] Heeman W, Calon J, van der Bilt A, et al. Dye-free visualisation of intestinal perfusion using laser speckle contrast imaging in laparoscopic surgery: a prospective, observational multi-centre study. Surg Endosc. 2023;37(12):9139-9146. https://doi.org/10.1007/s00464-023-10493-0
[31] Mannoh EA, Parker LB, Thomas G, et al. Development of an imaging device for label-free parathyroid gland identification and vascularity assessment. J Biophotonics. 2021;14(6):e202100008. https://doi.org/10.1002/jbio.202100008